Hindawi
Advances in Civil Engineering
Volume 2018, Article ID 9293623, 19 pages
https://doi.org/10.1155/2018/9293623

Research Article

An Investigation of Damage Mechanism Induced by Earthquake in a Plate Girder Bridge Based on Seismic Response Analysis: Case Study of Tawarayama Bridge under the 2016 Kumamoto Earthquake

Mya Nan Aye,[1] Akira Kasai,[2] and Mitsuhiro Shigeishi [2]

[1]*Graduate School of Science and Technology, Kumamoto University, Kumamoto 860-8555, Japan*
[2]*Faculty of Advanced Science and Technology, Kumamoto University, Kumamoto 860-8555, Japan*

Correspondence should be addressed to Mitsuhiro Shigeishi; shigeishi@civil.kumamoto-u.ac.jp

Received 28 February 2018; Revised 15 April 2018; Accepted 11 June 2018; Published 9 August 2018

Academic Editor: Mikayel G. Melkumyan

This paper reports a damage survey and seismic analysis of a bridge. In the first part, the damage survey of some bridges that were affected by the 2016 Kumamoto Earthquake was discussed. Among these bridges, the Tawarayama Bridge, which is a plate girder bridge located very close to an active fault line, was particularly considered. This bridge incurred severe damage because of the earthquakes' epicenters very close to the bridge. The damage mechanism that can occur in this type of bridge was elucidated. During the damage survey, parts of Tawarayama Bridge were examined to determine the damage in order to examine the factors of occurrence and damage mechanism. In the second part, the seismic responses of Tawarayama Bridge were analyzed using ABAQUS software, and beam elements were applied for the structural members. Firstly, the time-history responses were analyzed using both longitudinal and transverse direction earthquake ground motions separately and simultaneously to investigate the dynamic response of the bridge. Both undamped and damped conditions were considered. For the dynamic response analysis, the recorded earthquake acceleration data of Ozu Station were applied for both undamped and damped conditions considering both east-west (EW) and north-south (NS) directions simultaneously and the damped condition for these directions separately. In addition, a damped model was analyzed by applying design earthquake input data obtained from the Japanese Seismic Design Specifications for Highway Bridges. Consequently, five cases were established for seismic response analysis. Subsequently, the seismic responses of Tawarayama Bridge were investigated, and the behavior of the lower lateral members was examined considering the observed buckling of these members during the damage survey. The field survey and dynamic response analysis indicate that the buckling design of the lower lateral members should be considered in the future design of bridges.

1. Introduction

A series of earthquakes occurred in Kumamoto, Japan, in April 2016. The first earthquake with a magnitude of 6.5 (Japan Meteorological Agency (JMA) seismic intensity of 7) occurred on April 14. This earthquake was a foreshock, and it was followed by a mainshock with a magnitude of 7.3 (JMA seismic intensity of 7) on April 16. Within two days after the mainshock, more than 140 aftershocks, including at least 11 with a magnitude of 4.5 and one with a magnitude of 6, occurred in this region [1]. Mashiki town and Higashi Ward of Kumamoto were severely affected as the epicenters were located there. Many buildings and transportation infrastructures were damaged by these earthquakes. According to the records, the total fatality after the mainshock was 69 individuals, 364 individuals were seriously injured, and 1,456 suffered minor injuries, as of June 30, 2016. Overall, 8,044 buildings totally collapsed, 24,274 were half or partially destroyed, and 118,222 suffered moderate damage. Many bridges too were damaged [2, 3].

This study focuses on the damage incurred by bridges, especially plate girder bridges, during this series of earthquakes. Usually, buckling design is rarely considered in the design of lower lateral members of bridges. However, after the 2016

Kumamoto Earthquake, considering the observed buckling of the lower lateral members during the damage survey, concerns arose about the need for a buckling design for these members. It is essential to confirm the buckling of lower lateral members in a bridge by analytical methods to decide whether the buckling design of these members should be incorporated in future bridge designs. Therefore, a seismic response analysis of a plate girder bridge, whose lower lateral members underwent buckling, was carried out using the recorded earthquake motion data of the 2016 Kumamoto Earthquake.

The first section of this paper presented the introduction. The second one details the damage survey of bridges. The third one presents an overview of a plate girder bridge, namely, Tawarayama Bridge. The next two sections present the damage survey and seismic response analysis of Tawarayama Bridge. The response of the bridge subjected to the recorded motion of the 2016 Kumamoto Earthquake is then presented. Finally, some important findings and conclusions of the site survey and numerical analysis are presented.

2. Damage Survey of Bridges

2.1. Summary of Earthquake Data. According to the JMA, seven earthquakes with a high intensity (four with a magnitude of 5.4-5.9, two with a magnitude of 6.4–6.5, and one with a magnitude of 7.3) occurred in the same area between April 14 and 16. The epicenter was at Mashiki town in Kumamoto Prefecture [1].

Table 1 lists the time of occurrence, magnitude, and maximum seismic intensity of the largest earthquakes that occurred on April 14–16. Figure 1 shows a map presenting the locations of Kumamoto, Mashiki, and Mount Aso.

2.2. Overview of Bridge Damage. Among the 3,000 bridges in Kumamoto Prefecture, about 40 bridges, including Aso Bridge and Minami-Aso Bridge, were affected severely by the earthquake. Furthermore, 70 bridges under the Kumamoto Prefecture administration were damaged. In addition, the JR Kyushu Shinkansen (bullet train) was suspended because of the damage to the bridge on Kyushu Expressway. Although most bridge piers were not damaged after the foreshock, many bridges were severely damaged after the mainshock. In the Kumamoto region, pier settlement was the characteristic damage observed [2, 3]. Observation of the locations of damaged bridges on the map shows that most of these bridges were concentrated near faults, as shown in Figure 2 [4].

Bridges on Tawarayama Bypass, which is an important route connecting Kumamoto and Miyazaki Prefectures, were also damaged. Figure 2(a) is derived from an active fault database compiled by the National Institute of Advanced Industrial Science and Technology [4]. The thin red line at the center of the figure and the thick blue line show the Futagawa active fault and Prefectural Road No. 28, respectively. There are six bridges on Tawarayama Bypass; most of these bridges are curved bridges as the route passes through mountains. They were constructed in compliance with the 1996 version of specifications for highway bridges.

Table 1: Time of occurrence, magnitude, and maximum seismic intensity [1].

Time of occurrence	Magnitude	Maximum seismic intensity
4/14 21:26	6.5	7
4/14 22:07	5.8	6 (lower)
4/15 00:03	6.4	6 (upper)
4/16 01:25	7.3	7
4/16 01:45	5.9	6 (lower)
4/16 03:55	5.8	6 (upper)
4/16 09:48	5.4	6 (lower)

2.3. Overview of Damage to Ookirihata Bridge. Ookirihata Bridge is a five-span continuous curved bridge with a total length of 265.4 m. Girders supported by laminated rubber bearings and rubber joint load bearings are used as end supports. During this large-scale earthquake, the laminated rubber bearings underwent shear destruction, and the girder experienced a relative displacement of about 70 cm in the transverse direction. The main girder section prevented direct contact (collision) in the abutment parapet, preventing damage to the superstructure. This can be clearly seen in Figure 3(a). Figure 3(b) shows that a large step occurred at the expansion joint of Ookirihata Bridge [2, 3]. The bridge collapse-prevention cable was also deformed in a direction perpendicular to the bridge's axis. This led to rupture, and the girder fell down from its rubber bearing. This situation is depicted in Figure 3(c).

2.4. Overview of Damage in Other Bridges. Among the damaged bridges, Aso Bridge and Furyo First Bridge, situated on the prefectural road across the Kyushu Expressway, collapsed totally. Aso Bridge collapsed because of a huge landslide, about 710 m high, with a dip angle of 33°. Figures 4(a) and 4(b) show the collapse of Aso Bridge and Furyo First Bridge, respectively.

Some bridges, such as Hatanaka Dai-ichi Bridge, had to be urgently demolished. In Hatanaka Dai-ichi Bridge, the tops of piers completely collapsed, as shown in Figure 5. Figure 6 shows the damaged condition of Yokoe Bridge in Yatsushiro. In this bridge, the intermediate pier settled by about 2.3 m, causing the detachment of the bridge and sidewalk stairs [2, 3].

3. Overview of Tawarayama Bridge

Tawarayama Bridge is located on Prefectural Road No. 28, which is a route connecting Takamori with the vicinity of the downtown area of Kumamoto city center. It is a three-span girder bridge with a total length of 140 m, a maximum span length of 61.5 m, and an effective width of 8.5 m. The substructure consists of inverted T-type abutments (A1 and A2) and overhung piers (P1 and P2), and the foundation consists of caisson piles. The location of Tawarayama Bridge is shown in Figure 7. Figure 8 shows the longitudinal profile of the bridge. Figure 9 shows the plan view of the bridge; here, A1 represents the abutment on the Kumamoto side and A2 represents that on the Takamori side.

Furthermore, in the plan view, piers P1 and P2 represent the piers on the Kumamoto side and Takamori side,

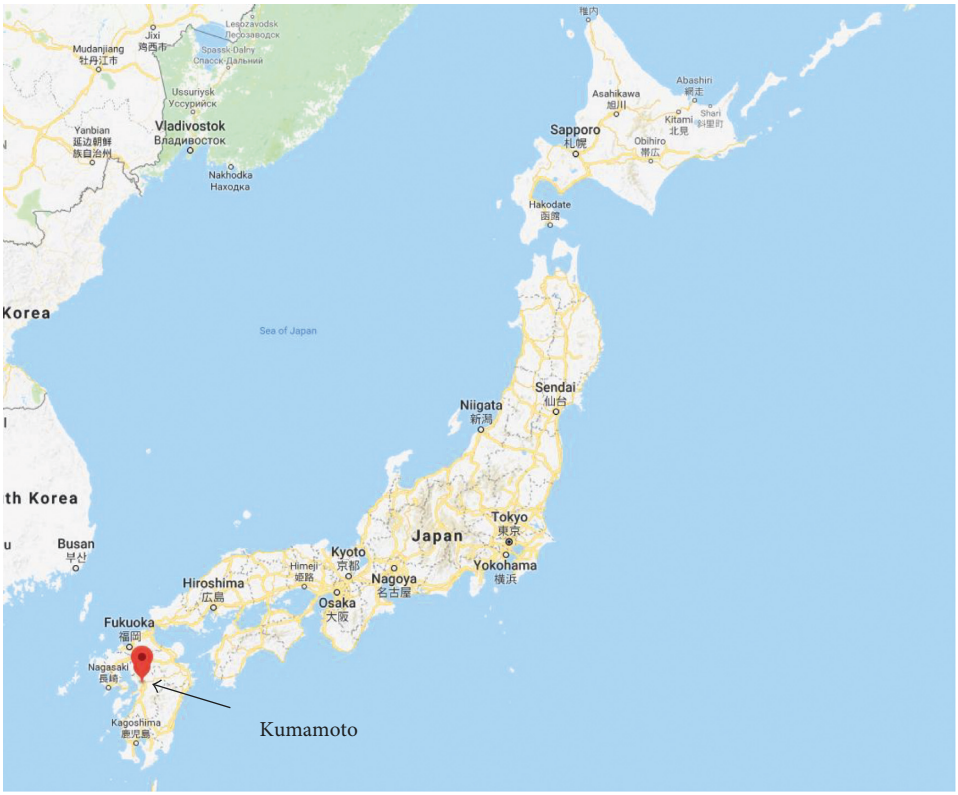

(a)

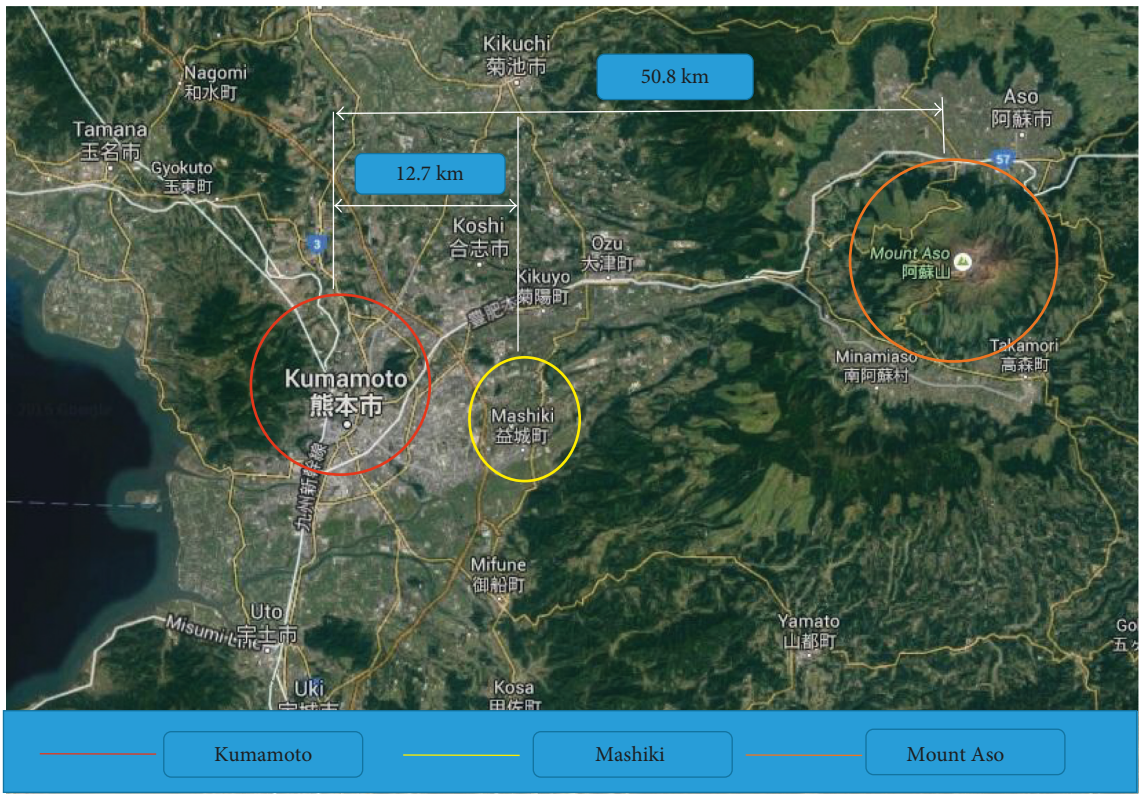

(b)

Figure 1: (a) The location of Kumamoto. (b) Distances between Kumamoto and Mashiki and Mount Aso. Source: https://www.google.co.jp.

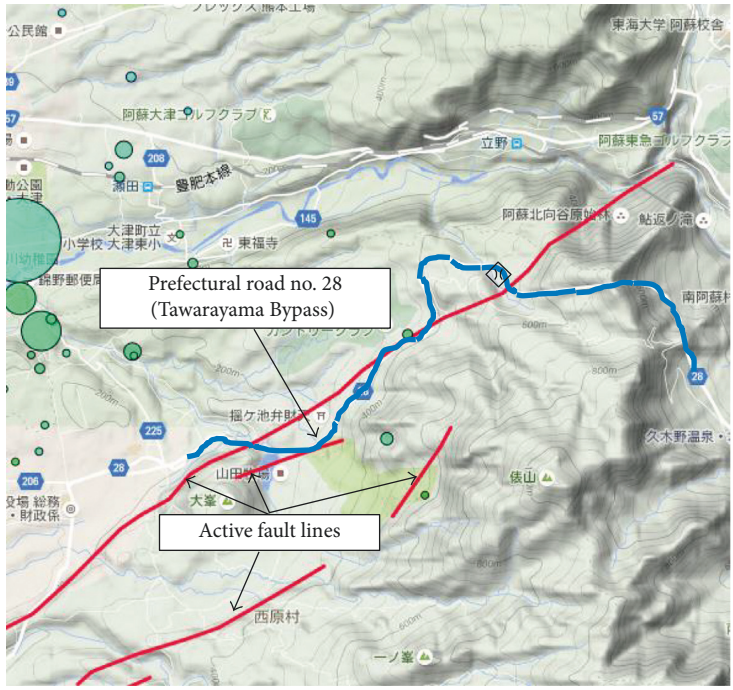

(a)

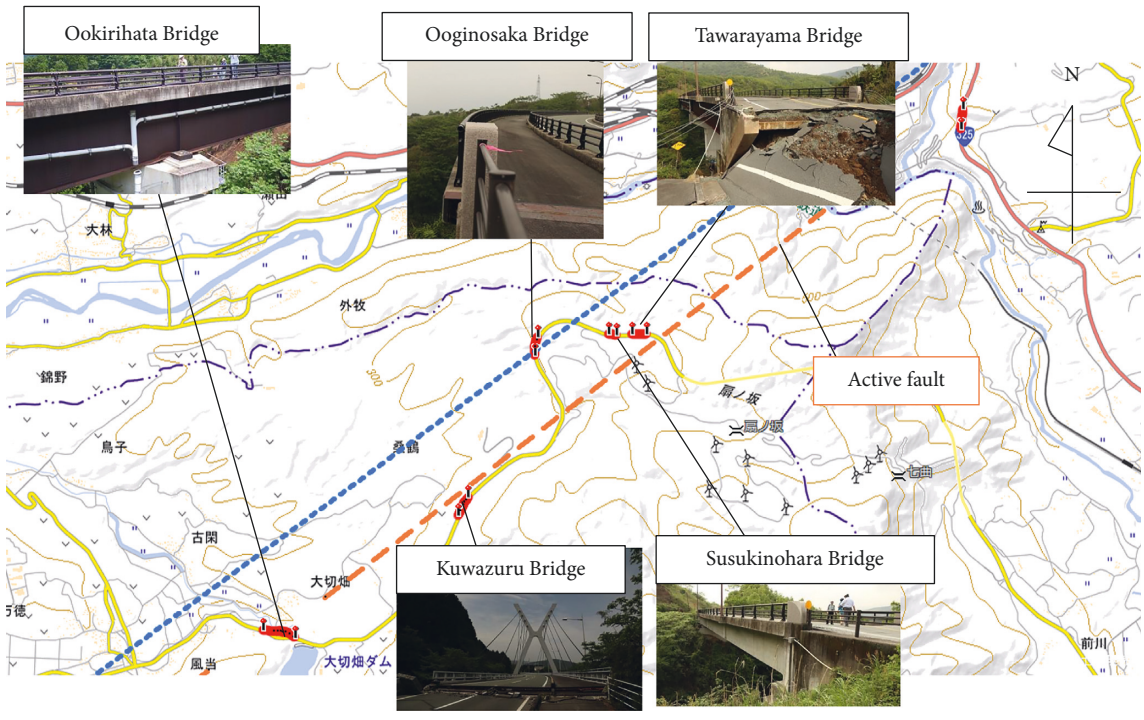

(b)

Figure 2: (a) Futagawa fault [4]. (b) Tawarayama Bypass and locations of bridges.

respectively. Figure 10 shows a cross section of the superstructure. Abutments A1 and A2 are constructed as single columns with a deep foundation. The bridge is nearly straight and has a cable-type girder collapse-prevention structure, which connects the girder and the bridge abutment parapet. Rubber bearings are used, and side blocks are provided at the girder ends only.

4. Site Survey of Tawarayama Bridge after the Earthquake

A site survey of Tawarayama Bridge was carried out. The damage was investigated by the Structural Mechanics Laboratory of Kumamoto University, led by Professor Toshitaka Yamao and Professor Akira Kasai, as the bridge was seriously

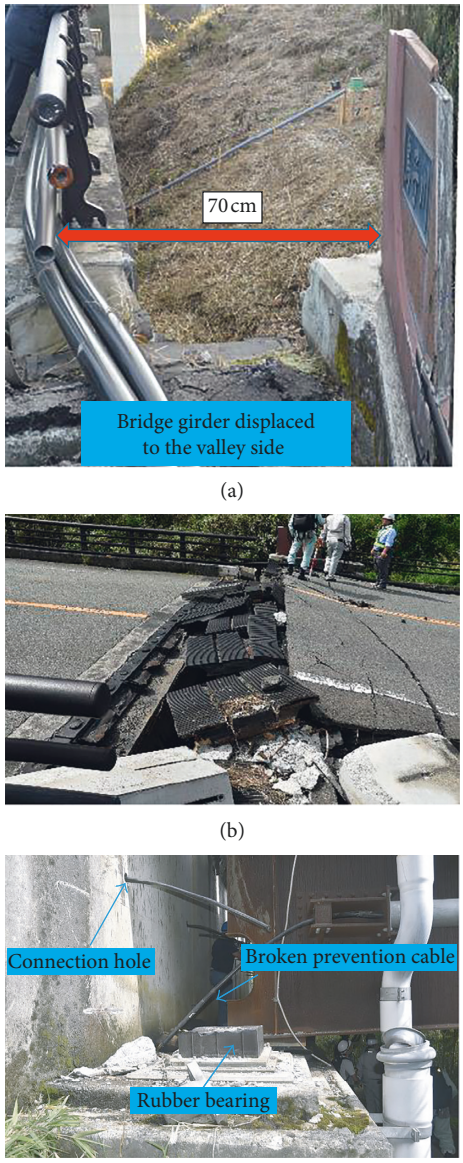

Figure 3: (a) Relative displacement of the girder, (b) damage to the expansion joint, and (c) damage to the bearing in Ookirihata Bridge.

damaged owing to its proximity to the active fault line. The deformation of the whole bridge can be seen in Figure 11, which was generated using a three-dimensional (3D) scanning technique that was developed by Yuta Ushitsuka.

According to the site survey data, all piers and abutments moved in the NE direction, and the movement and settlement of each abutment and pier were as follows:

(i) Abutment 1 moved 1,759 mm toward Takamori and 1,924 mm toward the valley and underwent a settlement of 410 mm.

(ii) Pier 1 moved 1,369 mm toward Takamori and 1,201 mm toward the valley.

(iii) Pier 2 moved 680 mm toward Takamori and 1,006 mm toward the valley.

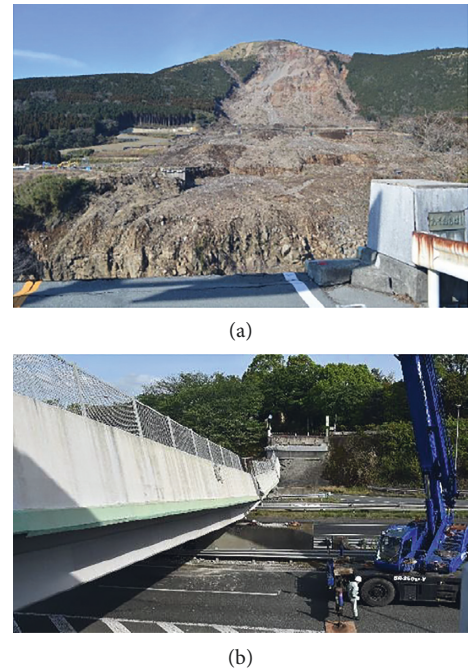

Figure 4: The collapse of (a) Aso Bridge and (b) Furyo First Bridge.

Figure 5: Damage to the tops of the piers of Hatanaka Dai-ichi Bridge.

Figure 6: Damage and detachment of the bridge and sidewalk stairs of Yokoe Bridge.

(iv) Abutment 2 moved 501 mm toward Takamori and 769 mm toward the valley.

The settlements of each bridge's abutments and piers are shown in Figure 11(c).

Figure 7: Location of Tawarayama Bridge.

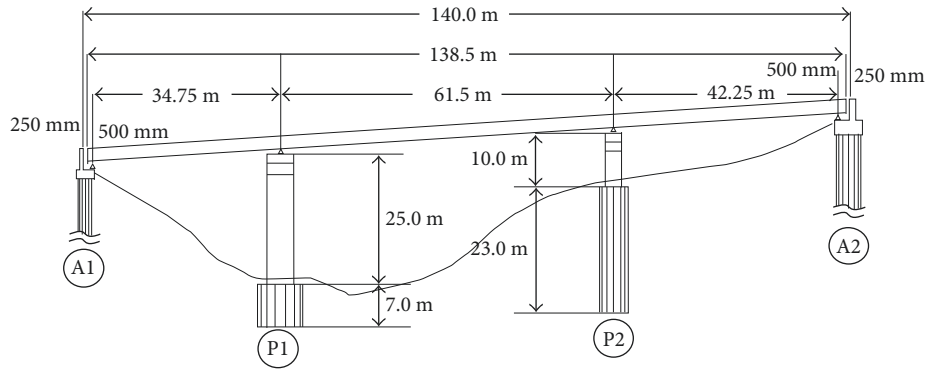

Figure 8: Longitudinal profile.

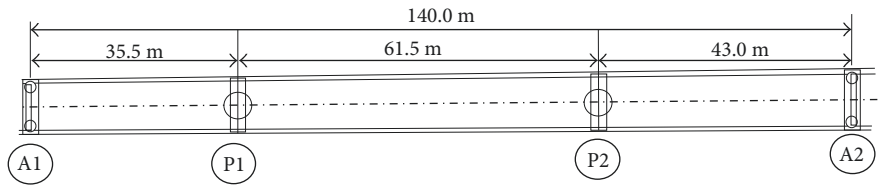

Figure 9: Plan view.

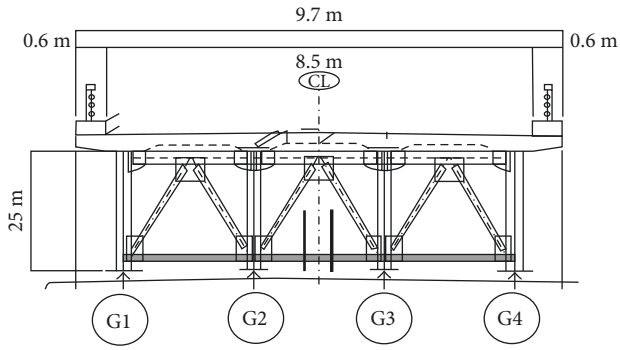

Figure 10: Cross section of the superstructure.

4.1. Damage at Abutments. The settlement of the deck slab occurred at the east side (A2 side) of the bridge because of the girders falling off from the rubber bearings and tilting of the abutment. A deck slab settlement of 53 cm was observed (Figure 12). The movement of the abutment by about 80 cm toward Takamori and the falling of the girder from the rubber bearing at abutment A2 are shown in Figure 13.

At the west side (A1 side, Figure 14), the road embankment collapsed because of the soil movement, exposing the pile foundation under the abutment. The base of abutment A1 was severely damaged, as shown in Figure 15. The shear deformation of the rubber bearing at abutment A1 is clearly seen in Figure 16.

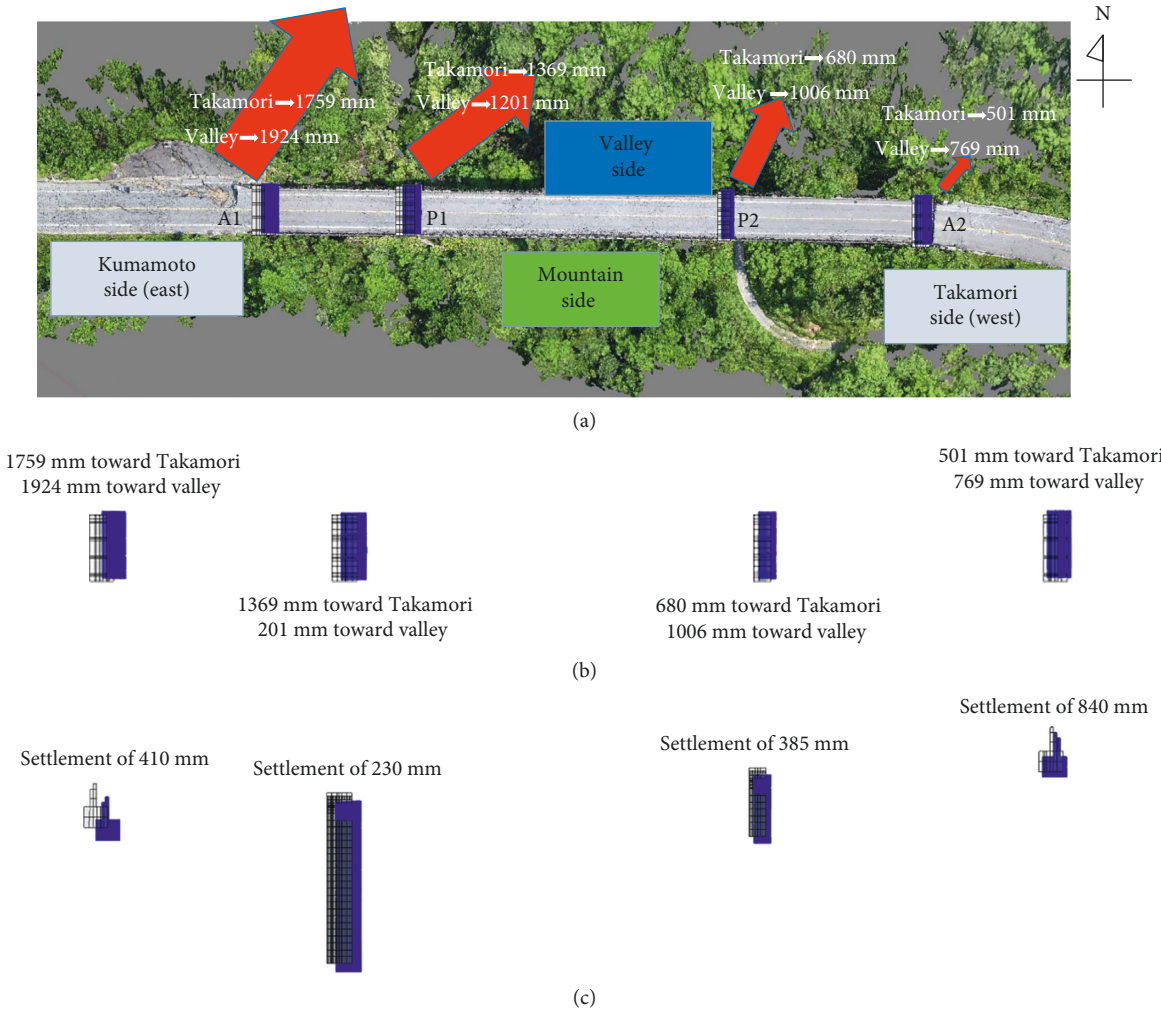

Figure 11: (a) Overall deformation of Tawarayama Bridge, (b) horizontal displacement of abutments and piers, and (c) settlement of abutments and piers.

Figure 12: Damage to abutment A2 (exterior).

(a)

(b)

Figure 13: Damage to abutment A2 (interior).

Figure 14: Damage to abutment A1 (exterior).

Figure 15: Damage to abutment A1 (interior).

4.2. Damage to the Piers. The rubber bearings at P2 were seriously damaged. One of the four rubber bearings under girder 1 completely collapsed. Many cracks that formed at the base of the pier were investigated. The following figures show the damage to the rubber bearing and the cracks that formed at the base (Figures 17–19).

(a)

(b)

Figure 16: Damage to the dampers at abutment A1 (interior).

(a)

(b)

Figure 17: Damage to the piers.

4.3. Damage to Girders. Figure 20 shows the deformation of the main girder and pier P1 as seen from the A1 side. The main girder bent and underwent inward deformation about 20 m from the A1 side while moving toward P1. Bucking in the vicinity of the lower lateral structure was confirmed near P1 and P2. The deformation of girder G3 is shown in Figure 21.

(a)

(b)

Figure 18: (a) Deformed rubber bearing under girder 1 at pier 2. (b) A rubber bearing that fell on the ground.

Figure 19: Cracks at the base of the pier.

4.4. Damage Mechanism. Figure 22 shows the original and deformed shapes of Tawarayama Bridge. The dotted line shows the original shape, and the solid line shows the deformed shape.

According to the damage survey presented in Sections 5.1–5.3, the impinging of the lower horizontal members buckling may be attributed to the compressive force acting on the bridge deck from both abutments A1 and A2 or to the displacement of the abutments toward the bridge girder. Figure 23 illustrates the deformation mechanism of the main girder and lower lateral members.

In this study, this event is considered the most important destructive mechanism. The extent of the compressive force that should be assumed for the seismic design of the bridge girder has not been verified yet. In addition, the actual ground motion was larger than what was assumed. Therefore, there is a need to identify the ground motion at the sites. According to this survey, in the future, the seismic design of bridge girders should be considered on the basis of the buckling phenomenon of these girders in response to ground motion corresponding to a seismic intensity of 7.

5. Seismic Response Analysis

There were many papers concerning the seismic response analysis, seismic design specification of the bridges, and damages of bridges published by many researchers. Aso et al. [5] carried out nonlinear earthquake response analysis of PC cable-stayed bridge. Nazmy [6] presented seismic analysis and design evaluation of continuous plate-girder bridges with the help of a case study. Itani et al. [7] emphasized on seismic behavior of steel girder bridge superstructures to know the behavior of steel plate girder bridges during the earthquakes. Park et al. [8] simulated the seismic performance subjected to near-fault ground motion. Usami et al. [9] performed dynamic analysis to evaluate the seismic performance of steel arch bridges against major earthquakes. Kawashima and Unjoh [10] summarize the seismic design specifications for highway bridges after the 1995 Kobe Earthquake. Altın et al. [11] carried out dynamic analysis of suspension bridges and full-scale testing in which the effects of large deflections are taken into account. Takahashi and Hoshikuma [12] explored the damages of road bridges induced by the ground motion in the 2011 Great East Japan Earthquake and summarized the characteristics of damage to road bridges induced by the ground motion. Cahya et al. [13] also investigated seismic response behavior using static pushover analysis and dynamic analysis of half-through steel arch bridge under strong earthquake. The 2016 Kumamoto Earthquake survey report published by the Asia-Pacific Economic Cooperation [14] and an overview of damage to roads and bridges in Nishihara area by Narazaki and Kong [15] presented the damage conditions of bridges during the 2016 Kumamoto Earthquake. There was a research on the collapse process of cable-stayed bridges under strong seismic excitations by Wang et al. [16]. According to all these research works, it is obvious that the seismic response analyses and seismic design specifications of bridges as well as damage survey of bridges are essential. So, in the present study, a seismic response analysis of a plate-girder bridge, whose lower lateral members underwent buckling, was carried out using the recorded earthquake motion data of the 2016 Kumamoto Earthquake. ABAQUS (Simulia, 2017) software [17] was used to create a finite element (FE) model of Tawarayama Bridge. In this model, beam elements were used to study the buckling behavior. According to the design drawing sheets, L-, T-, I-beams were used for cross-bracing, top and bottom chords, and cross-beams, respectively. For rubber bearings, spring elements were applied in the FE model. The material properties of the model used in the numerical analysis were SM490 with a yield stress (σ_y) of 315 MPa and a Young's modulus (E) of 205 GPa for the main girder steel beams, SMA400w with a yield stress (σ_y) of 245 MPa and a Young's modulus (E) of 205 GPa for all bracing members, and concrete with a Young's modulus (E) of 30.35 GPa.

The nonlinearity of the material was considered for the steel elements, which are the main elements of the

(a)

(b)

Figure 20: Deformation of the main girders and buckling of the lower lateral members.

Figure 21: Deformation of girder 3.

plate girder and lower lateral members. Beam elements were used for concrete piers. The equivalent Young's modulus was used to account for steel reinforcements too. The equivalent Young modulus used for P1 and P2 is 36.18 GPa and 38.14 GPa, respectively. In the present study, the elastic linear hardening model was used to consider the elastoplastic behavior of steel. The elastic linear hardening models of SM490 and SMA400w grade steels are shown in Figure 24 [18, 19]. The FE model created using ABAQUS CAE software is shown in Figure 25.

Beam type B31 (two-node linear beam) was used in the FE model. Spring elements were installed between piers and girders in all six directions to represent the rubber bearings in the real bridge. Dashpot coefficients were also applied, and the equation used and values are shown in the next section. A detailed calculation of the spring stiffness is presented in the next section. Multipoint constraint (MPC) beam type was used between the girders and connections of the bracing members.

5.1. Calculation of Spring Stiffness from the Properties of Rubber Bearings. In the FE model of Tawarayama Bridge, spring elements were used for rubber bearings between girders and piers and abutments. The following formulae were used to calculate the spring stiffness in the model [20].

For the horizontal direction,

$$K_{so} = \frac{G_0 A}{\sum t_e},$$
$$K_{st} = \frac{G_0 A}{\sum t_e}. \quad (1)$$

For the vertical direction,

$$K_v = \frac{EA}{\sum t_e},$$
$$E = \begin{cases} (3 + 6.58S^2) & \text{for } \left(0.5 \le \frac{b}{a} \le 2\right), \\ (4 + 3.29S^2) & \text{for } \left(\frac{b}{a} < 0.5 \text{ and } \frac{b}{a} > 2\right), \end{cases} \quad (2)$$
$$S = \begin{cases} \frac{ab}{(2(a+b)t_e)} & \text{for } \left(0.5 \le \frac{b}{a} \le 2\right), \\ \frac{a}{2t_e} & \text{for } \left(\frac{b}{a} < 0.5 \text{ and } \frac{b}{a} > 2\right), \end{cases}$$

where K_{so}, K_{st}, and K_y are the spring stiffnesses in the horizontal and vertical directions, G_0 is the shear modulus, A is the area of the rubber bearing, t_e is the thickness of the laminated rubber, E is Young's modulus, S is the shape factor, a is the width of the rubber bearing, and b is the length of the rubber bearing.

The springs were installed at A1, P1, P2, and A2 between abutments or piers and girders. At each abutment and pier, four springs are installed under each girder. The values of each parameter used and the calculated spring stiffnesses are listed in Table 2.

5.2. Seismic Input Data. The recorded earthquake data from Ozu Station were used as seismic input data. The earthquake acceleration waves for the north-south (NS) and east-west (EW) directions are shown in Figures 26 and 27 [21]. The maximum acceleration occurred around 26 s in both directions. The values and times of occurrence are also shown in the figures. For Tawarayama Bridge, EW is the longitudinal direction and NS is the transverse direction. Both directions were considered to investigate the seismic

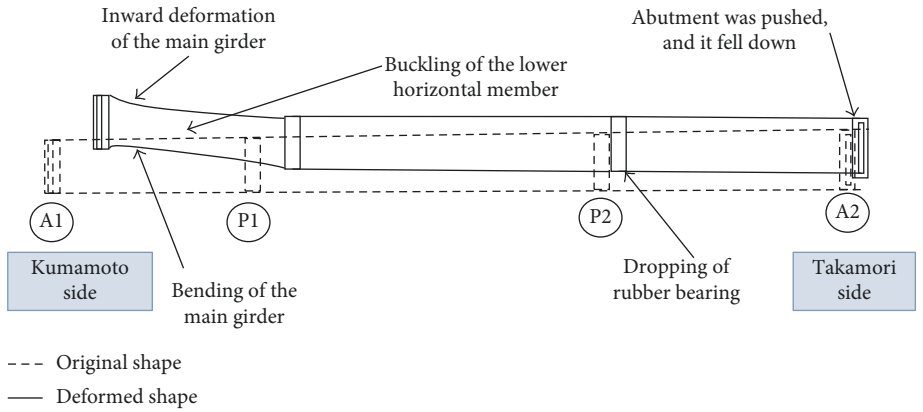

Figure 22: Deformation mechanism of the whole bridge.

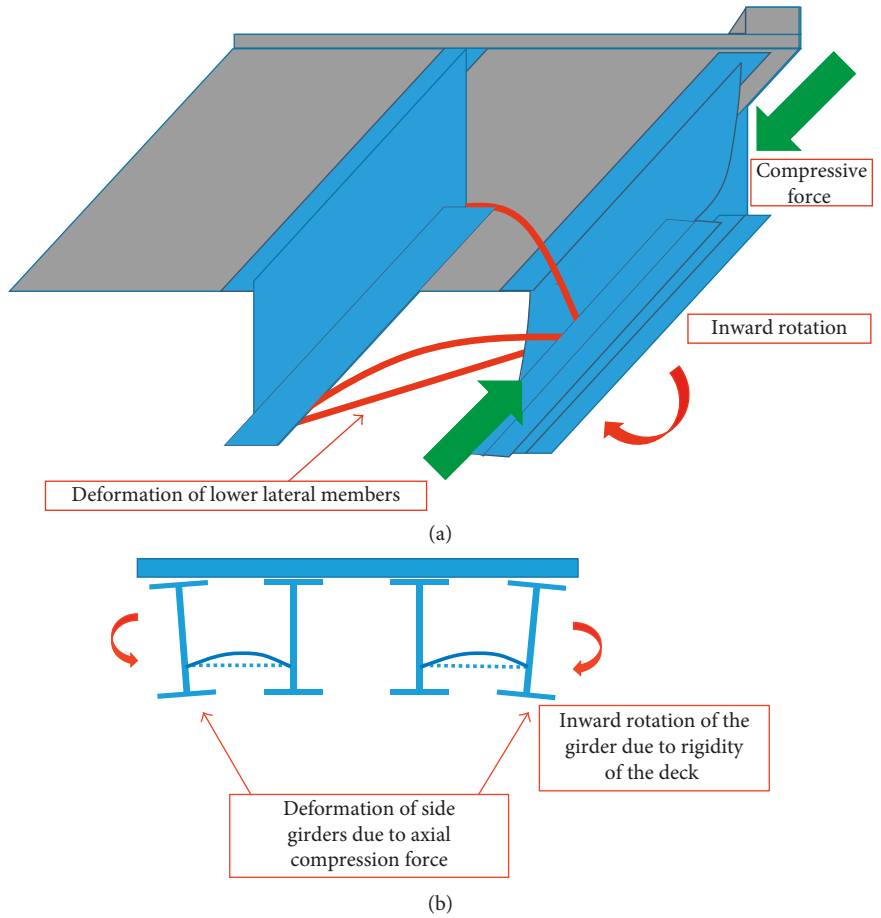

Figure 23: Deformation mechanism of the main girder and lower lateral members.

response of the bridge. In addition to the recorded earthquake data, analyses using the design earthquake data, considering level II, type II ground, ground motion type I, were also carried out [1, 20].

5.3. Numerical Analysis. For the numerical analysis, a constant time step of 0.01 s was utilized. MPC beam constraints were applied for the contacts between the members. The model was assumed to have no residual stresses and no initial crookedness modes. The elastoplastic behavior of the steel material was considered during the analysis. First, an eigenvalue analysis was carried out in order to understand the vibration characteristics of the bridge. The values of the Rayleigh damping coefficients, α and β, as determined from this analysis, are 0.6 and 0.002, respectively, for concrete and 0.11 and 0.0005, respectively, for steel materials. The seismic response analysis with a ground acceleration input and a constant dead load was

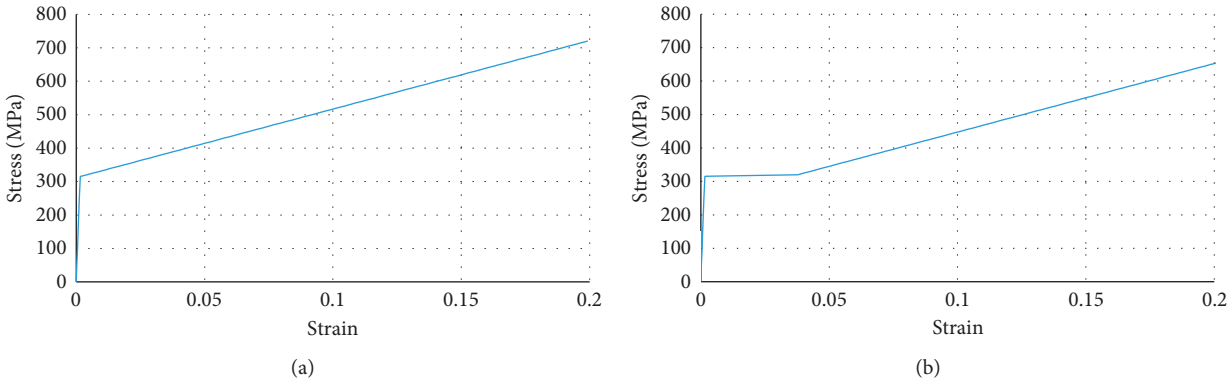

Figure 24: Stress-strain relationship for (a) SM490 and (b) SMA400w grade steels.

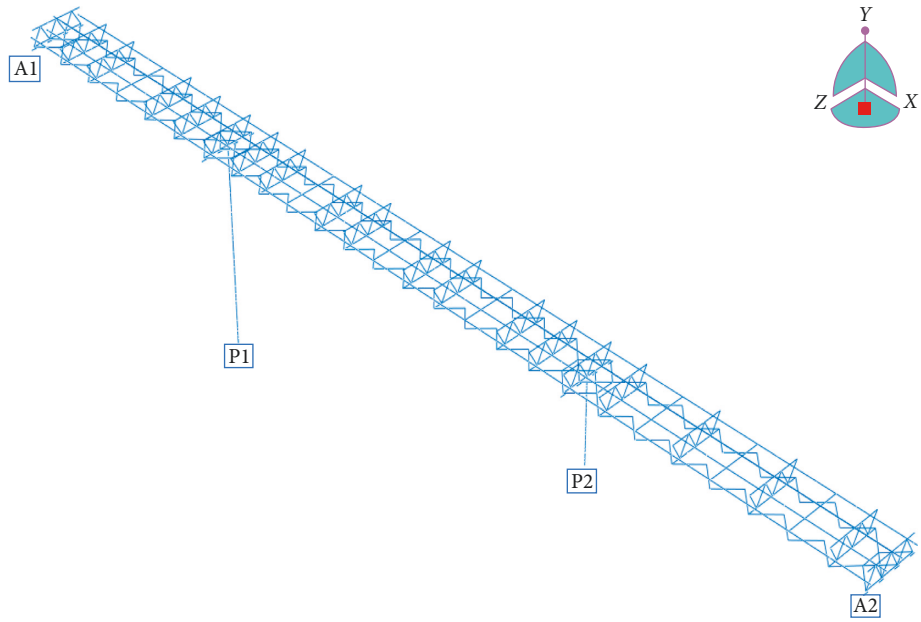

Figure 25: FE model of Tawarayama Bridge.

performed using the FEM ABAQUS program, which can account for geometric and material nonlinearities. In the analysis, both undamped and damped conditions were applied. For the undamped model, both transverse and longitudinal earthquake waves were applied simultaneously. For the damped model, three cases were examined. In the first case, the earthquake wave was applied only in the EW direction. In the second one, the wave was applied only in the NS direction. Finally, in the last one, the wave was applied in both longitudinal and transverse directions. In addition to Ozu Station data, level II, type II ground, ground motion type I, and earthquake data were also applied under the damped condition, and both EW and NS directions were considered in the analysis. The dashpot coefficients, c, that were used in the analysis are listed in the following Table 3. The dashpot coefficient equation used is as follows [17]:

$$c = \frac{2k\xi}{\omega}, \tag{3}$$

where c is the dashpot coefficient, k represents stiffness, ξ is the damping ratio, and ω is the natural frequency.

6. Seismic Response Behavior of the Plate Girder Bridge

The seismic response behaviors of the plate girder bridge will be discussed in this session for four different parts. First, the stress states in the lateral bracing members are presented, and then, the behavior of the spring is discussed. Thereafter, the trajectory curves of the piers are illustrated. Finally, the behavior of the lower lateral bracings is examined.

6.1. Stress States in the Lateral Bracing Members. The stress states of all lateral bracing members for all five cases are presented in this section. The locations of all bracings are shown in Figure 28, and the stress states and maximum stress locations are shown in Figure 29.

Table 2: Properties of the rubber bearings and spring stiffnesses.

Part	G_0 (N/mm^2)	a (mm)	b (mm)	A (mm^2)	t_e (mm)	n	$\sum t_e$ (mm)	S	E (N/mm^2)	K_{so} (Nm/mm)	K_{st} (tf/cm)	K_v (tf/cm)
A1	0.785	450	450	202500	12	17	204	9.375	456.064	794.117	794.117	461637
P1	1.177	600	650	390000	22	5	110	7.091	392.883	4252.54	4252.54	1420410
P2	1.177	750	750	562500	36	3	108	5.208	213.555	6250	6250	1134190
A2	0.785	450	450	202500	13	11	143	8.654	388.961	1132.87	1132.87	561661

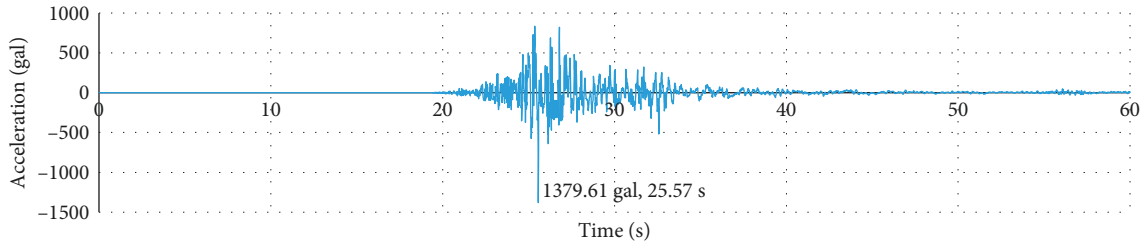

Figure 26: Earthquake input acceleration wave in the NS direction.

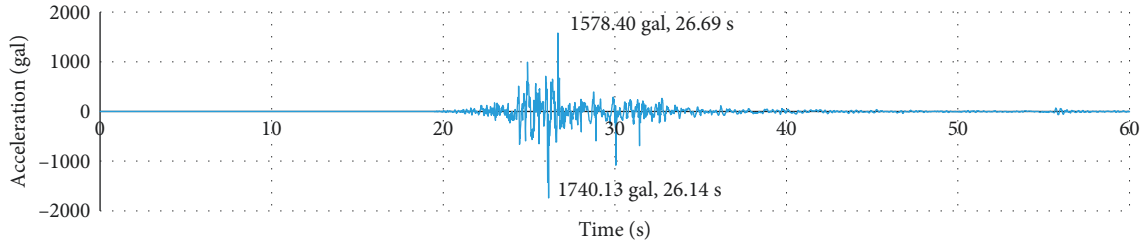

Figure 27: Earthquake input acceleration wave in the EW direction.

Table 3: Dashpot coefficients, c, for each abutment and pier.

	(A1, dir 1,3)	(A1, dir 2)	(A2, dir 1,3)	(A2, dir 2)	(P1, dir 1,3)	(P1, dir 2)	(P2, dir 1,3)	(P2, dir 2)
k	794.117	461637	1132.87	561661	4254.54	$1.43E+06$	6250	$1.13E+06$
c	15.88234	9232.74	22.6574	11233.22	85.0908	28528.2	125	22683.8

The present bridge has a total of 394 lateral bracing members. Among them, 66 members in the undamped case, 16 members in the design earthquake (EQ) case, and six members in the EW and NS case exceed the σ/σ_y value of 1, and for the EW case and NS case, the σ/σ_y value of no members exceeds 1. For each of the abovementioned cases, the number of members whose σ/σ_y values are between 0.8 and 1 is 100, 13, 2, 5, and 10, respectively. The σ/σ_y values of other members are less than 0.8. The maximum σ/σ_y value is 1.59 in the undamped case. Detailed data are listed in Table 4. The member with the maximum σ/σ_y value is an inclined member of P-bracing (bracing at piers) between G1 and G2. Most of the members with σ/σ_y values close to 1.5 are found near P1 and P2 (P-bracing and bottom bracing). The σ/σ_y values of most of the bracings and A-bracing members are less than 0.8. The minimum σ/σ_y value of 0.02 was found at A-bracing (bracing at abutments).

6.2. Deformation of the Spring Element. This section discusses the deformation of the spring elements, which were used as rubber bearings in the bridge. Springs were installed at 16 locations (four for each pier and abutment) between the girder and piers/abutments, which are shown in Figure 30. Figure 31 presents the load-displacement relationship curves of a spring at P2 under the undamped condition in both longitudinal and transverse directions. The dotted lines in the figure show the theoretical displacement criteria of spring elements.

The theoretical displacement criteria of spring elements for each pier and abutment are listed in Table 5.

The displacement of all springs in all cases except in the undamped case was within their displacement criteria. In the undamped case, the displacement of springs at A2, P1, and P2 in the longitudinal direction and that of P2 in the transverse direction exceed the displacement criteria. The maximum displacement of springs occurred between 25.5 s and 26.8 s, which is close to the time when the maximum acceleration occurred.

At A1 and P1, displacements of the springs in the transverse direction are greater than those in the longitudinal direction for the design EQ case and NS case, whereas

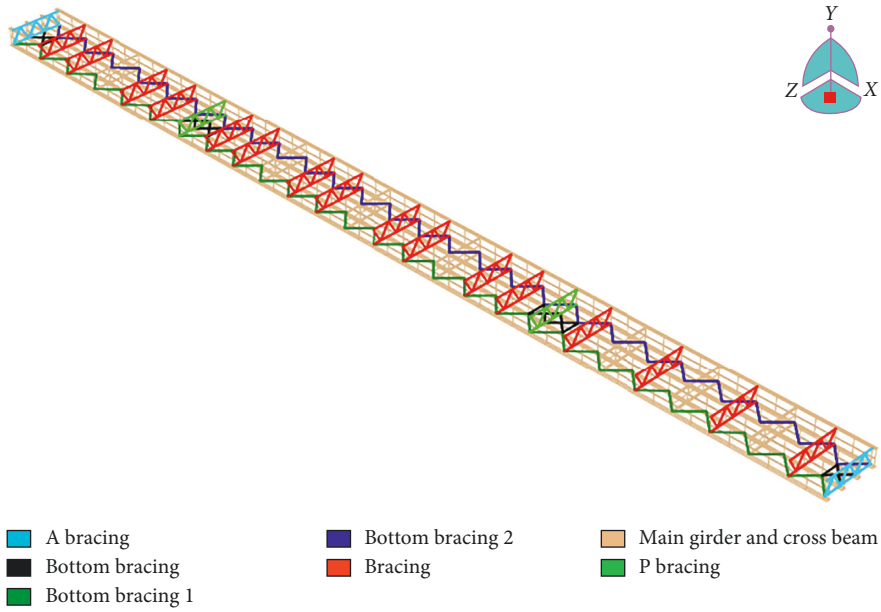

Figure 28: Locations of bracings.

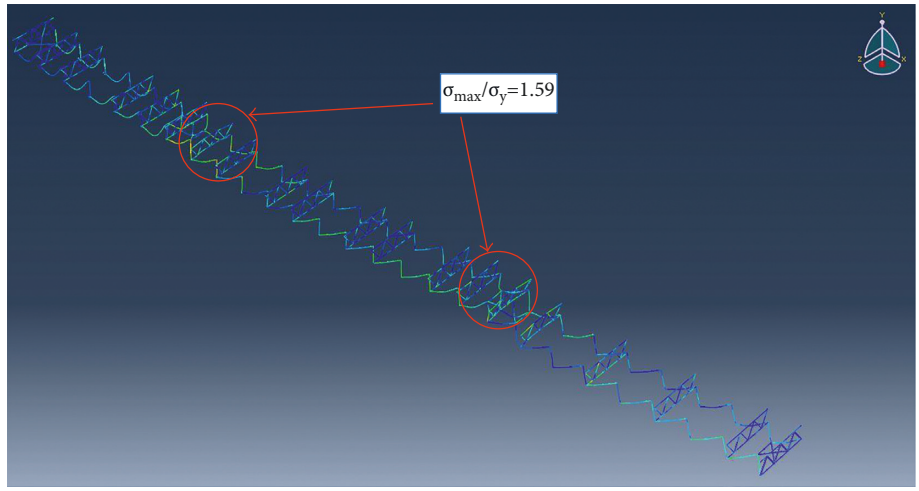

Figure 29: Members with the maximum σ/σ_y value.

Table 4: Number of members according to σ/σ_y values.

σ/σ_y value	Undamped	Design EQ	EW	NS	EW and NS
$\sigma > 1$	66	16	0	6	0
$0.8 < \sigma \leq 1$	100	13	2	5	10
$\sigma < 0.8$	228	365	392	383	384
Max. σ	1.59	1.2	0.85	1.2	0.97

the longitudinal displacements of the springs are more dominant in the other cases. For A2 and P2, the maximum spring displacements in the longitudinal direction are greater than those in the transverse direction in all other cases, except for the NS case. The ratio of longitudinal to transverse displacements of P2 for EW and NS cases is 1.9, which is larger than the values of others (around 1). This fact and the fact that the spring displacement of P2 exceeds the displacement criteria in both longitudinal and transverse directions may be the reason why one of the rubber bearings at the P2 pier fell down. The displacements of springs in the longitudinal and transverse directions for all cases are shown in Figure 32.

6.3. Trajectory Curve of Piers. The trajectory curves of piers were established in order to determine their response during the earthquake. These curves are shown in Figure 33. Among the five cases, the undamped case is more dominant, followed by the design earthquake one. It is clear that the displacements in the EW (longitudinal) and NS (transverse) directions are only dominant in their respective direction for both P1 and P2. The undamped displacements of both piers are more dominant in the

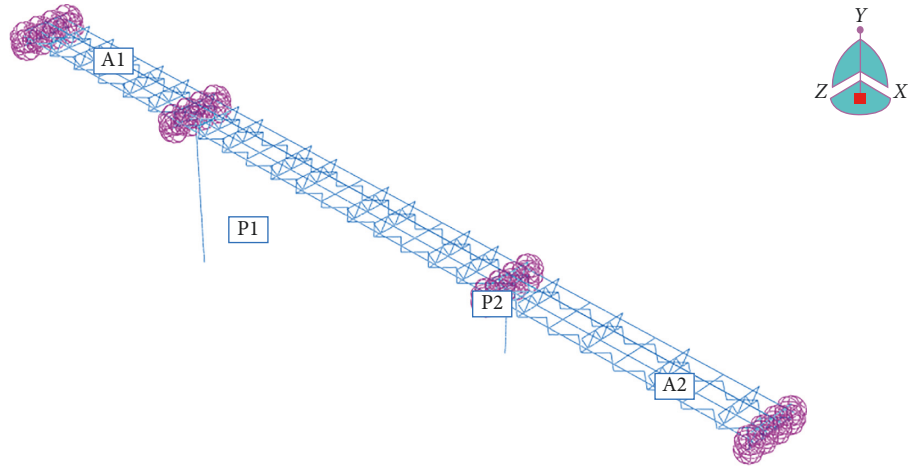

Figure 30: Location of springs.

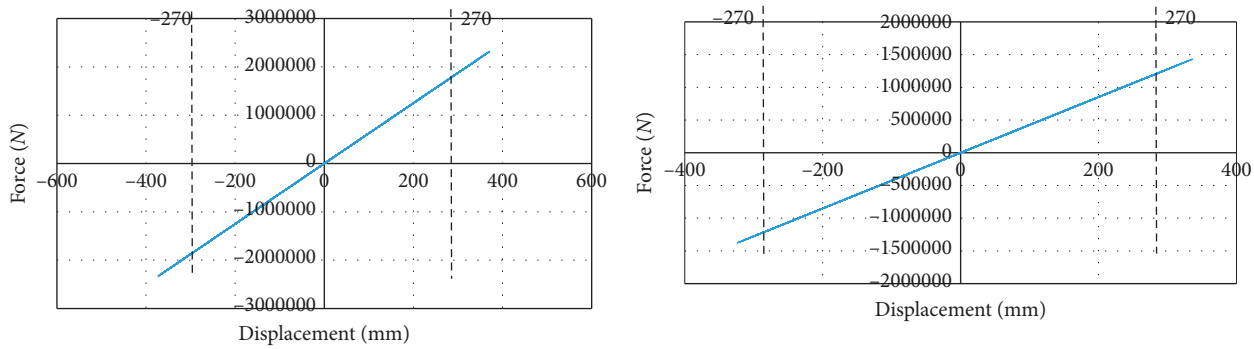

Figure 31: Force-displacement curves for the spring at pier 2.

Table 5: Displacement criteria of spring elements.

Pier/abutment	Displacement criteria (mm)
Pier 1	275
Pier 2	270
Abutment 1	510
Abutment 2	375

transverse direction. The design EQ displacements are also dominant in the transverse direction, although they are not very different from the undamped displacement, whereas the EW and NS displacements are nearly identical in both directions.

6.4. Behavior of Lower Lateral Bracings. The time history displacement response curves and force-displacement curves of some lower lateral bracing members were plotted in order to understand the behavior of lower lateral bracing members. The stresses of some of these members exceeded the maximum stresses, leading to hardening. Hence, some members exhibited an elastoplastic behavior, whereas some exhibited an elastic behavior only. Among the ten selected members shown in Figure 34, eight members buckled in the undamped case, five buckled in the design EQ, and two each buckled in the EW and the EW and NS cases. In the NS case, no member buckled. Figure 35 shows that the members around P2 have a greater tendency to buckle, especially under the damped condition.

The lengths of the members, maximum forces, Euler's buckling load, and buckling conditions for the undamped case are listed in Table 6. The buckling conditions for all bracing members for each case are presented in Table 7. No member buckled only in the EW case. In all the other cases, members exhibited a buckling behavior under earthquake motion. These data imply that the damper plays an important role in the buckling of members.

7. Discussion and Conclusion

In this study, field surveys of Tawarayama Bridge were conducted in order to review the actual conditions and damage mechanism that could have caused the deformation observed in the first part of this study. According to this damage survey, the following conclusions can be drawn.

(1) A large ground motion occurred near Tawarayama Bridge. This led to the movement of the entire

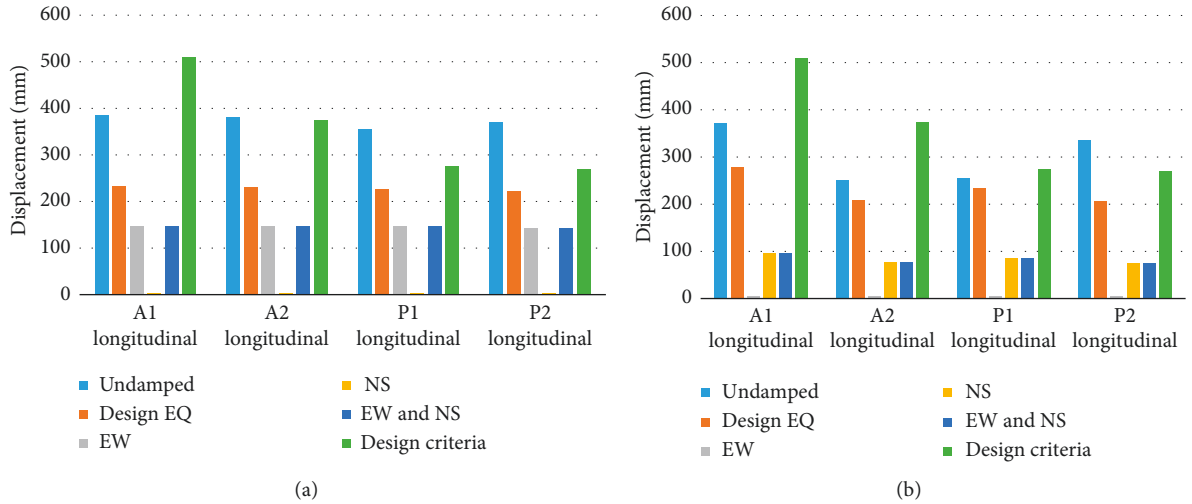

Figure 32: Spring displacement of the spring in each abutment and pier for all cases: (a) longitudinal direction and (b) transverse direction.

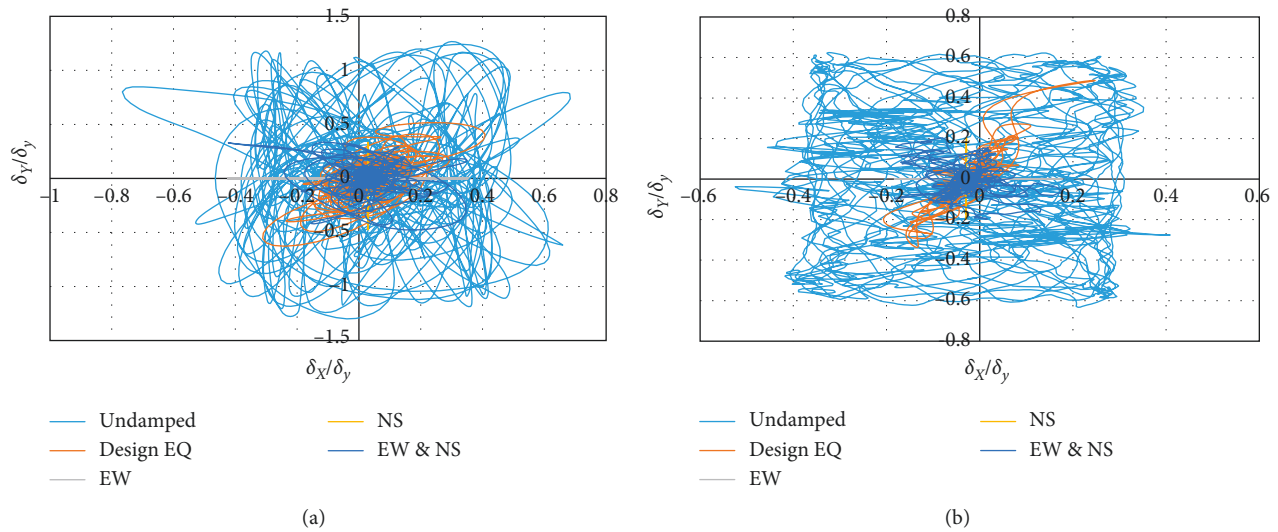

Figure 33: Trajectory curve for (a) pier 1 and (b) pier 2.

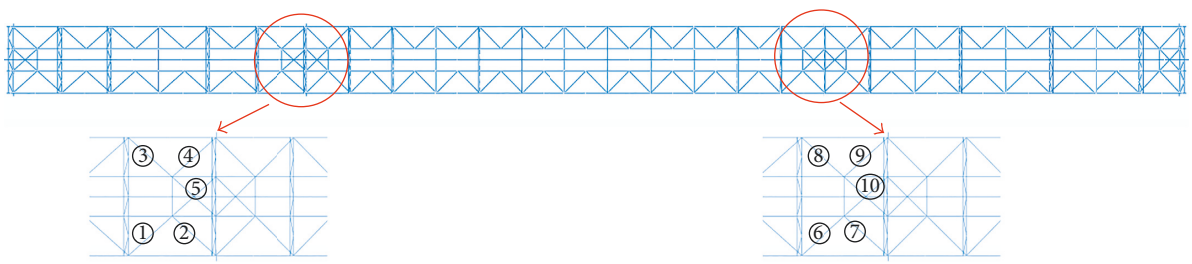

Figure 34: Locations of the buckled lower bracing members.

bridge in the NE direction (toward Takamori side in the longitudinal direction and toward the valley in the transverse direction). As a result, a large compressive and rotational force acted on the bridge girder.

(2) The lower lateral members buckled, and the rubber bearings underwent shear deformation. The movements were much larger in A1 and P1, and so the deformations of the bridge girder in both the flange and the web could be clearly seen.

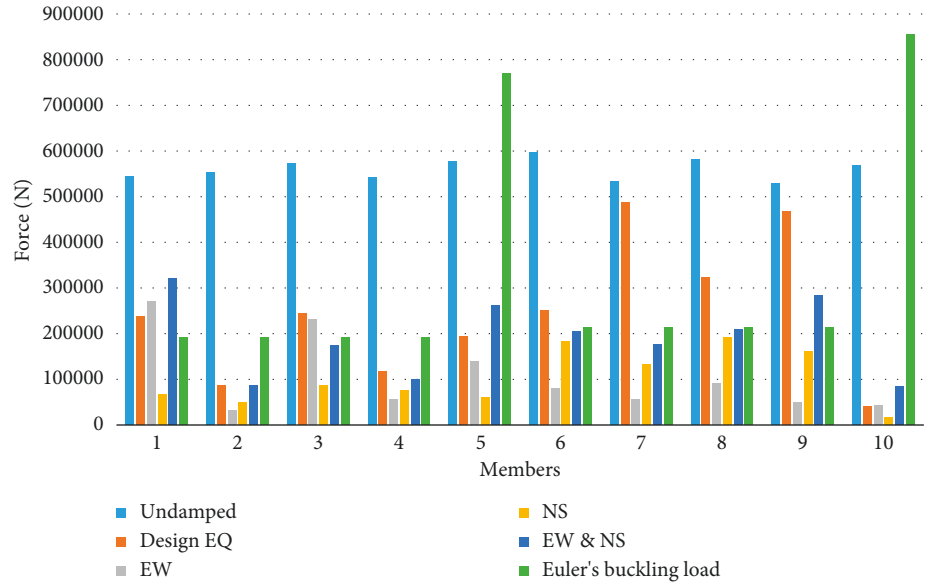

Figure 35: Maximum forces and Euler's buckling forces for each case.

Table 6: Buckling conditions of ten selected members under the undamped condition.

Member	1	2	3	4	5	6	7	8	9	10
Length (mm)	3895	3895	3895	3895	1947	3695	3695	3695	3695	1847
Max. force (N)	543107	552285	571835	541638	577698	597243	532315	581386	528864	567483
Euler's buckling load (N)	192618	192618	192618	192618	770471	214057	214057	214057	214057	856228
Buckle or not	Buckle	Buckle	Buckle	Buckle	Not buckle	Buckle	Buckle	Buckle	Buckle	Not buckle

Table 7: Buckling conditions of all members in different earthquakes.

	Undamped	Design EQ	EW	NS	EW and NS
Number of buckled members	66	16	0	6	39
Number of unbuckled members	100	378	394	388	355

(3) Extensive damage occurred in every abutment and pier. The most serious damage included the exposure of the pile foundation and shear deformation of rubber bearings at abutment A1, the tendency of overturning of abutment A2, buckling at P1, and the falling off of one of the four rubber bearings at P2.

(4) The possible damage mechanism may be attributed to the compressive force acting on the bridge deck from both abutments A1 and A2 or to the approaching of the abutments toward the bridge girder.

The second part of the study was a numerical analysis of Tawarayama Bridge. The numerical analysis is subdivided into eigenvalue analysis and seismic response analysis subject to the ground motion. The seismic analysis was carried out with the earthquake acceleration input data for longitudinal and transverse directions separately and simultaneously in order to investigate the seismic behavior of the bridge. The current findings and conclusions of these analyses are summarized as follows:

(1) According to the eigenvalue analysis, the displacement in the transverse direction is dominant in mode 1, whereas that in the longitudinal direction is clear in mode 3. The movements of the bridge in both directions occurred in the real situation too. In mode 2, a vertical rotation is noticeable. This behavior is similar to the rotation of the bridge girder toward the valley side during the 2016 Kumamoto Earthquake.

(2) The relative stresses in most bracing members are lower than 0.8 when considering the earthquake input data in only one direction. For the recorded bilateral earthquake input data of Ozu Station, the relative stresses of ten members exceeded 0.8 and those of the other members were below 0.8. For design earthquake data, the σ/σ_y values of 16 members exceeded 1, those of 13 members exceeded 0.8, and those of the rest were less than 0.8. For the undamped model, the numbers of the members with σ/σ_y exceeding 1 and 0.8 were 66 and 100, respectively.

(3) While observing the displacement of springs, which represent the rubber dampers in the actual condition, spring displacements beyond the displacement criteria can be found only in the undamped case, especially for the springs at P2.

(4) The performance of piers differs according to the cases. For the undamped and design earthquake cases, displacement in the transverse direction is dominant, and for the EW and NS case, displacements in both directions are quite similar. The displacements in the EW and NS case are dominant in their respective directions. Among the five cases, the undamped cases are dominant.

(5) No buckling behavior is observed in the EW case, whereas six members buckled in the NS case. It is observed that some members exhibit a buckling behavior even in the design earthquake case. Overall, 39 members buckled under the recorded earthquake motion in the EW and NS directions. Here, 66 members buckled during the analysis under the undamped condition. In the real situation, it was confirmed that the rubber bearings underwent shear deformation, and one rubber bearing from P2 fell off. The buckling of lower lateral members was also clearly observed.

(6) Thus, it can be concluded that the buckling of the lower lateral members should be given due importance in further bridge designs, especially for bridges with lower damping.

In the present work, only the recorded acceleration was considered as the input data for dynamic analysis, and large geometric deformations and bridge collapse-prevention cables were not considered. So, further studies should include these facts as analysis input data to obtain more accurate results.

Data Availability

The data used to support the findings of this study are available from the corresponding author upon request.

Disclosure

This paper is an extension of the work reported in the paper titled "Damage survey of bridges during 2016 Kumamoto Earthquake and seismic response analysis of plate girder bridge subjected to the Kumamoto Earthquake," presented at the International Workshop on the 2016 Kumamoto Earthquake–Japan-US Joint Workshop on March 6, 2017, at Fukuoka, Japan. The previous paper emphasized on the damage survey and eigenvalue analysis, and the present paper also includes the nonlinear dynamic analysis responses.

Conflicts of Interest

The authors declare that they have no conflicts of interest.

Acknowledgments

The authors would like to express their sincere gratitude to Professor Toshitaka Yamao for his leadership and guidance during the site survey of Tawarayama Bridge. Special thanks are due to Yuta Ushitsuka for helping to obtain the 3D image for the deformation of Tawarayama Bridge by 3D scanner technique.

References

[1] *Data from JMA (Japan Meteorological Agency)*, 2016, http://www.data.jma.go.jp.

[2] A. K. Tang and J. M. Eidiner, *Kumamoto, Kyushu, Japan, Earthquake of Mw 6.0 April 14, 2016, Mw 7.0 April 16, 2016, Lifetime Performance*, The Council of Lifeline Earthquake Engineering TCLEE No. 2 and Yokohama National University, Yokohama, Japan, 2017.

[3] http://www.eqclearinghouse.org.

[4] https://gbank.gsj.jp/activefault/index_gmap.html.

[5] T. Aso, K. Mizutori, M. Shuto, A. Arikado, K. Momota, and H. Otsuka, "Non-linear earthquake response analysis of PC cable stayed bridge considering the fluctuant axial force," in *Proceedings of the 12WCCE (12th World Conference on Earthquake Engineering)*, Auckland, New Zealand, February, 2000.

[6] A. S. Nazmy, "Seismic analysis and design evaluation of continuous plate-girder bridges: a case study," *International Journal of Structural Stability and Dynamics*, vol. 3, no. 1, pp. 91–106, 2003.

[7] A. M. Itani, M. Bruneau, L. Carden, and I. G. Buckle, "Seismic behavior of steel girder bridge superstructures," *Journal of Bridge Engineering*, vol. 9, no. 3, pp. 243–249, 2004.

[8] S. W. Park, H. Ghasemi, J. Shen1, P. G. Somerville, W. P. Yen, and M. Yashinsky, "Simulation of the seismic performance of the Bolu Viaduct subjected to near-fault ground motions," *Earthquake Engineering and Structural Dynamics*, vol. 33, no. 13, pp. 1249–1270, 2004.

[9] T. Usami, Z. Lu, H. Ge, and T. Kono, "Seismic performance evaluation of steel arch bridges against major earthquakes, Part 1: dynamic analysis approach," *Earthquake Engineering and Structural Dynamics*, vol. 33, no. 14, pp. 1337–1354, 2004.

[10] K. Kawashima and S. Unjoh, "Seismic design of highway bridges," *Journal of Japan Association for Earthquake Engineering*, vol. 4, no. 3, pp. 174–189, 2004.

[11] S. Altın, K. Kaptan, and S. S. Tezcan, "Dynamic analysis of suspension bridges and full scale testing," *Open Journal of Civil Engineering*, vol. 2, no. 2, pp. 58–67, 2012.

[12] Y. Takahashi and J. Hoshikuma, "Damage to road bridges induced by ground motion in the 2011 Great East Japan Earthquake," *Journal of JSCE*, vol. 1, no. 1, pp. 398–410, 2013.

[13] E. Cahya, T. Yamao, and A. Kasai, "Seismic response behavior using static pushover analysis and dynamic analysis of half-through steel arch bridge under strong earthquake," *International Journal of Civil Engineering and Technology (IJCIET)*, vol. 5, no. 1, pp. 73–88, 2014.

[14] Asia-Pacific Economic Cooperation, "2016 Kumamoto earthquake survey report," in *Proceedings of the 10th Emergency Preparedness Working Group Meeting*, pp. 15-16, Lima, Peru, August, 2016.

[15] Y. Narazaki and C. Kong, *Overview of Damage to Roads and Bridges in Nishihara Area*, 2016, http://www.eqclearinghouse.org/2016-04-15-kumamoto/2016/05/19/overview-of-damage-to-roads-and-bridges-in-nishihara-area/.

[16] X. Wang, B. Zhu, and S. Cui, "Research on collapse process of cable-stayed bridges under strong seismic excitations," *Shock and Vibration*, vol. 2017, Article ID 7185281, 18 pages, 2017.

[17] Dassault Systèmes Simulia Corp., *ABAQUS 6.14 Documentation*, Dassault Systèmes Simulia Corp., Providence, RI, USA, 2014.

[18] W. F. Chen, *Plasticity for Structural Engineers*, Springer, Berlin, Germany, 2012.
[19] Japan Road Association, *Handbook of Road Bridge Bearing*, Japan Road Association, Tokyo, Japan, 2004.
[20] Japan Road Association, *Specifications for Highway Bridges, Part I–General, Part II–Steel Bridges, Part V–Seismic Design*, Japan Road Association, Tokyo, Japan, 2012.
[21] http://www.kyoshin.bosai.go.jp/, 2016.